Title

Heterobinuclear Light Absorber Coupled to Molecular Wire for Charge Transport across Ultrathin Silica Membrane for Artificial Photosynthesis

Journal

ACS Applied Materials & Interfaces, 10(37)

ISSN

1944-8244

Authors

Katsoukis, Georgios

Frei, Heinz

Publication Date

2018-09-19

DOI

10.1021/acsami.8b11684

Peer reviewed

Heterobinuclear Light Absorber Coupled to Molecular Wire for Charge Transport across Ultrathin Silica Membrane for Artificial Photosynthesis

Georgios Katsoukis and Heinz Frei*

Molecular Biophysics and Integrated Bioimaging Division, Lawrence Berkeley National Laboratory, University of California, Berkeley, CA 94720

HMFrei@lbl.gov

(*ACS Appl. Mater. Interfaces*, accepted)

Keywords: Artificial photosynthesis, silica membrane, charge transfer, molecular wire, surface anchoring, transient optical spectroscopy

Abstract

Coupling of robust, all-inorganic heterobinuclear light absorbers to metal oxide catalysts for water oxidation across an ultrathin product-separating silica membrane requires charge transfer through organic molecular wires embedded in the silica. A synthetic approach for assembling the bimetallic units on the silica surface is introduced that is compatible with the presence of encapsulated organic molecules. Accurate selection and fine tuning of the concentration of embedded conducting wires is enabled by a two-step method consisting of surface attachment of a tripodal anchor, trimethoxy silyl aniline, followed by attachment of *p*-oligo(phenylene vinylene) through amide linkage. Each step of the assembly process was monitored and characterized by a combination of FT-IR, FT-Raman and UV-Vis spectroscopy. Hole transfer was observed from transient Co^{III}, formed by $Ti^{IV}OCo^{II} \rightarrow Ti^{III}OCo^{III}$ charge transfer excitation of the chromophore, to *p*-oligo(phenylene vinylene) molecule within the 8 nanosecond width of the photolysis laser pulse by the transient optical absorption spectroscopy of the wire radical cation. The rectifying property of the light absorber-wire assembly enabled by appropriate selection of redox potentials of metals and embedded wire obviates the need for a molecularly defined linkage between the components. Combined with the previously observed ultrafast hole injection from the embedded wires to Co oxide catalyst, the result implies visible light induced hole transfer from visible light excited binuclear light absorber to water oxidation catalyst across the silica separation membrane in a few nanoseconds or faster. Demonstration and understanding of this interfacial charge transfer step is critical for developing nanoscale core-shell architectures for complete photosynthetic cycles.

1. Introduction

All-inorganic molecularly defined light absorbers such as ZrOCo units anchored on a silica surface, when coupled to metal oxide nanoparticle catalysts for water oxidation, have recently been shown to accomplish photocatalytic reduction of CO_2 by H_2O to CO and O_2 at the gas-solid interface.[1] Hence, this polynuclear unit affords closing of the photosynthetic cycle of CO_2 reduction by H_2O on the nanoscale. Direct coupling of other oxo-bridged heterobinuclear units with nanoparticle catalysts has been demonstrated, e.g. $TiOCr^{III}$ driving IrO_2 cluster for water oxidation,[2] or ZrOCo coupled at the Zr center to Cu_xO_y nanocatalyst for CO_2 reduction.[3] The robust light absorbers, of which a dozen different units with mostly first row transition metals have been introduced thus far [4-7] enable close matching of the redox potential of donor and acceptor metal center with the potential of the water oxidation or carbon dioxide reduction catalyst, respectively, which is essential for achieving conversion of a maximum fraction of the absorbed solar photon energy to chemical energy of the product.

For developing artificial photosystems that convert CO_2 and H_2O to more deeply reduced products, preferably a liquid hydrocarbon, separation of the incompatible oxidation and reduction catalysis environments by a membrane is required to minimize efficiency-degrading back and cross reactions. To this end, our design is a metal oxide-silica core-shell nanotube array in which each nanotube operates as a complete, independent photocatalytic unit.[4,5,8] In its current version, the core is a Co_3O_4 nanotube of 0.5 μm diameter and wall thickness of 10 nm.[8] The inside of the Co oxide tube provides the surface for water oxidation catalysis while the outside is covered by a 2 nm thick amorphous silica shell featuring embedded molecular wires. This SiO_2 membrane readily transmits protons but is impermeable to small molecules including O_2. Embedded organic wire molecules (*p*-oligo(phenylene vinylene) featuring 3 aryl units) afford

charge transport from the heterobinuclear light absorber anchored on the outer surface across the ultrathin silica membrane to the Co oxide catalyst on the inside. Fabrication of the core-shell nanotube array has been demonstrated,[8] and charge and proton transport across the silica membrane quantified and mechanistically investigated by transient optical and photoelectrochemical methods.[9-13] Short circuit photocurrent measurements demonstrated that charge transfer across the silica membrane is tightly controlled by the orbital energetics of the embedded wire molecule.[9] Application of these new membranes has been expanded to nanoscale integration of other types of incompatible catalytic environments such as inorganic with microbial catalysts.[14]

Spectroscopic investigation of charge transfer requires selection of a suitable morphology of the core-shell construct to achieve adequate sensitivity for the specific technique at hand. For time resolved optical spectroscopy, experiments with spherical Co_3O_4-SiO_2 core-shell nanoparticles in the form of aqueous colloids allowed us recently to uncover sub-ps hole transfer from a visible light absorber on the outside of the silica shell to the embedded molecular wire followed by transfer to the Co_3O_4 catalyst within 250 ps.[10] However, monitoring of charge transport through embedded molecular wires across the silica membrane by ultrafast optical spectroscopy required the use of familiar organometallic light absorbers because analysis of the spectra was only feasible for chromophores with established ultrafast spectroscopic signature,[10] not yet available for the heterobinuclear chromophores. Hence, a critical step is to explore the coupling of heterobinuclear light absorbers with metal oxide catalyst for water oxidation across the ultrathin silica separation membrane via embedded molecular wires.

Here, we demonstrate charge transfer from a binuclear light absorber, $TiOCo^{II}$, anchored on the outside of spherical core-shell nanoparticles to silica-embedded *p*-oligo(phenylene

vinylene) wires by transient optical absorption spectroscopy. These experiments were enabled by the development of new synthetic methods for molecular wire attachment and for assembly of the MMCT unit that afford substantially improved control of loading level and anchoring of binuclear light absorbers without harming the embedded organic molecules. It is shown that the rectifying property of the light absorber-wire assembly, made possible by the flexible choice of redox potentials of metals and wire obviates the need for molecularly defined linkage between the components. This interfacial charge transfer step is critical for exploring complete core-shell assemblies for closing the photosynthetic cycle on the nanoscale under membrane separation.

2. Experimental Section

Synthetic Materials and Methods

All chemicals were purchased from Sigma-Aldrich including HPLC grade (99.8%) solvents, which were dried with 3Å molecular sieve (Alfa-Aesar) for three days and stored in a nitrogen glovebox before use, unless noted otherwise. Hole conducting molecular wires of type *oligo*-para(phenylene vinylene) consisting of three units (abbreviated PV3) asymmetrically functionalized with one sulfonyl group on one end and one carboxy group on the opposite end, namely, Cesium 4-((E)-4-((E)-4-sulfonatostyryl)styryl)benzoate ($Cs_2PV3\_SO_3\_CO_2$), were synthesized according to the general methods described in previous work.[12]

Anchoring of 4-(Trimethoxysilyl)aniline on SiO_2 nanoparticles (SiO_2/TMSA): 1.0 g (16.4 mmol) of SiO_2 (silica nanopowder, specific surface area 175-225 m^2/g, 99.8 %, 12 nm diameter) were dispersed in 200 mL toluene by ultrasonication and subjected to vigorous stirring for 1 h

before adding 94.7 mg (0.44 mmol) of 4-(Trimethoxysilyl)aniline (TMSA) (Gelest, 90% (10% 3-(Trimethoxysilyl)aniline)) and heating at 100˚C. After 24 h, 3 mL of deionized water was added to the suspension while keeping the solution at 100˚C for another 3 h. After cooling to ambient conditions the suspension was filtrated and the residue was rinsed with tetrahydrofuran (30 mL), ethanol (30 mL), and hexane (30 mL) and dried in an oven at 115˚C to afford SiO_2/TMSA powder with surface coverage of 12 $\pm$ 2 %, corresponding to 0.3 TMSA anchor nm^{-2} on average (see SI for details of surface coverage calculations).

Synthesis of tris(hydroxymethyl)aminomethane, anchoring on SiO_2 nanoparticles (SiO_2/tripod): Tris(bromomethyl)aminomethane hydrobromide (TBAM) was synthesized according to literature.[15] 1 g of SiO_2 (16.4 mmol) was dried under vacuum at 100˚C for 1 h before refilling with N_2 and adding 120 mL of acetonitrile (Honeywell). 58.7 mg (0.15 mmol) of TBAM was added to the suspension under vigorous stirring together with 22.5 mg (0.3 mmol, 2 eq.) dry NaI and heated under reflux for 12 h. After cooling to ambient conditions the solvent of the brownish suspension was removed by rotovap, and the red/orange residue was redispersed in water (100 mL), filtrated and rinsed with water (50 mL) and ethanol (50 mL). After drying in vacuum, SiO_2/$(CH_2)_3CNH_2$ (abbrev. SiO_2/tripod) nanoparticles at 0.8% surface coverage were obtained as a white powder (0.02 nm^{-2}, upper limit estimate, see SI).

Covalent attachment of PV3_SO_3_CO_2 on SiO_2 particles (SiO_2/TMSA-PV3): All solid materials were dried in vacuum and kept under inert atmosphere prior to use. 1.0 mg (2.6 μmol, 1.05 eq.) of HATU (O-(7-Azabenzotriazol-1-yl)-N,N,N′,N′-tetramethyluronium-hexafluorphosphate) and 1.7 mg (2.5 μmol, 1.0 eq.) Cs_2PV3_SO_3_CO_2 were dissolved in 3 mL

dimethylformamide and stirred for 30 min. In parallel, a suspension of 100 mg SiO_2/TMSA in 5 mL DMF was prepared by ultrasonication for 30 min. The samples were mixed, and the resulting bright yellow cloudy and greenish fluorescent suspension was stirred for 7 days, converting to a pale yellow-blueish fluorescent suspension. The suspension was centrifuged (8,500 rcf, 20˚C, 1 h) and the colorless supernatant was decanted. The yellow residue was agitated in 15 ml water and centrifuged once more. The centrifugation-decantation procedure was repeated once with ethanol and once with hexane. The residue was then dried in vacuum at 120˚C to provide SiO_2/TMSA-PV3 as a fluorescent pale yellow material with a functionalization yield of 0.02 PV3 nm^{-2}.

Casting of anchored PV3 into silica (SiO_2/TMSA-PV3/SiO_2): An ultrathin silica layer was grown on SiO_2/TMSA-PV3 by a solvothermal method using tetraethyl orthosilicate (TEOS) as precursor. 20 mg of SiO_2/TMSA-PV3 particles were dispersed in a Teflon container in a mixture of 90 mL ethanol, 6 ml water, and 4 mL NH_4OH (30%) by ultrasonication and vigorous stirring for 30 min. 100 μL TEOS was added quickly and the suspension stirred for 24 h, after which it was centrifuged (8,500 rcf, 20˚C, 1 h) and the clear supernatant decanted. The white residue was agitated in 15 ml ethanol and twice centrifuged. The resulting product SiO_2/TMSA-PV3/SiO_2 was dried in vacuum at 120˚C for 24 h.

Anchoring of Ti^{IV} on SiO_2/TMSA-PV3/SiO_2 surface (SiO_2/TMSA-PV3/SiO_2/Ti^{IV}): Two methods were developed for anchoring Ti^{IV} centers onto SiO_2/TMSA-PV3/SiO_2 particles that leave the embedded wire molecules intact. In one approach, covalent attachment of Ti^{IV} centers on the outer silica shell surface was based on the previously employed titanocene dichloride

method [16,17] modified to avoid calcination at 550˚C that otherwise might damage the silica embedded organic wires. Briefly, 55 mg of SiO_2/TMSA-PV3/SiO_2 particles (915 μmol) were dehydrated in vacuum at 150 C for 3 h, put under Argon atmosphere and suspended in 30 mL dry methylene dichloride by ultrasonication for 30 min. 3.3 mg of titanocene dichloride (13.3 μmol, 0.015 eq.) was dried under vacuum at 120˚C for 1 h and held under Argon atmosphere, dissolved in 2 mL dry methylene dichloride and then added to the SiO_2/TMSA-PV3/SiO_2 suspension. The orange suspension was stirred for 15 min before adding 50 μL of triethylamine. After 12 h the suspension turned pale yellow. The suspension was centrifuged (8,500 rcf, 20˚C, 1 h) and the supernatant replaced twice with dichloromethane/ethanol = 5/1 mixture. The resulting dispersion was exposed to 405 nm (170 mW) continuous laser photolysis light for 45 min (Excelsior 405C-200-CDRH 200 mW continuous wave laser), centrifuged and the supernatant again replaced with dichloromethane/ethanol mixture. The photolysis procedure was repeated 3 times. The filtrated powder was redispersed in ethanol/H_2O = 5/1 h and the pH adjusted to 9 using 30% aqueous ammonia before vigorous stirring for 6 h at 50 C. The resulting pale yellow SiO_2/TMSA-PV3/SiO_2/Ti powder was dried in vacuum at 200˚C.

A second approach for covalent attachment of Ti^{IV} centers on the outer silica shell surface was conducted by using Tetrakis(diethylamido)titanium(IV) ($Ti(NEt_2)_4$, $Et=CH_2CH_3$) (Sigma-Aldrich; 99.999% trace metal basis) as precursor. 67.7 mg SiO_2/TMSA-PV3/SiO_2 nanoparticles were dried at 100˚C under high vacuum in a vacuum flask over night. The flask was transferred to an Argon glove box and was filled with 30 mL of anhydrous tetrahydrofuran and vigorously stirred for 10 min. 6 μl $Ti(NEt_2)_4$ were added to the suspension and stirring was continued for another 5 h. The resulting yellow material was centrifuged and the supernatant was replaced

twice with ethanol for centrifugation. The resulting material was then dried under high vacuum at 100˚C.

Linking of Co^{II} to Ti^{IV} on SiO_2/TMSA-PV3/SiO_2 (SiO_2/TMSA-PV3/SiO_2/$Ti^{IV}OCo^{II}$): The grafting of Co^{II} centers was performed as described previously.[17] In short, 30 mg of SiO_2/TMSA-PV3/SiO_2/Ti^{IV} (500 µmol) were dehydrated in vacuum at 200˚C for 3 h, rendered under Argon atmosphere and suspended in 30 mL dry acetonitrile by ultrasonication for 30 min. 1.0 mg of Cobalt(II) chloride (7.5 µmol, 0.015 eq.) was dried under vacuum at 120˚C for 1 h, exposed to an Argon atmosphere, dissolved in 2 mL dry acetonitrile and added to the SiO_2/TMSA-PV3/SiO_2/Ti^{IV} particle suspension. The blue suspension was stirred for 15 min before adding 10 µl of trimethylamine. Continued stirring for 12 h turned the color to pale blue. The suspension was centrifuged (8,500 rcf, 20˚C, 1 h) and the supernatant replaced twice with acetonitrile. The resulting light blue material SiO_2/TMSA-PV3/SiO_2/$Ti^{IV}OCo^{II}$ was dried in vacuum at 250˚C for 3 h. The same procedure was used for the preparation of SiO_2/TMSA-PV3/SiO_2/Co^{II} particles taking SiO_2/TMSA-PV3/SiO_2 as starting material.

Transient optical absorption spectroscopy: A nanosecond transient absorption spectrometer Edinburgh Instruments model LP920 equipped with a pulsed Xe probe lamp was used in conjunction with a Nd:Yag laser pumped tunable optical parametric oscillator (Continuum model Surelite II and Surelite OPO Plus) as excitation source. The laser pulse width was 8 ns, and measurements were conducted either at 1 Hz or 10 Hz repetition rate. Samples were pressed into self-supporting wafers with 18 mg of material under 10 ton of force in a 13 mm die held under

vacuum or Ar atmosphere in a quartz cuvette at 45 degree angle relative to perpendicular pump and probe beams.

Vibrational and optical spectroscopy: Samples for FT-IR and UV-vis transmission spectroscopy were placed in a home-built miniature stainless steel vacuum cell equipped with CaF_2 or KBr windows and evacuated for 2 hours.[1] Infrared spectra were recorded at 2 cm^{-1} resolution with Bruker spectrometers model Vector 33, IFS66V, or Vertex 80V equipped with liquid nitrogen cooled MCT detectors. FT-Raman spectra of powders were measured with the FRA-106 Raman accessory of the IFS66V spectrometer at 2 cm^{-1} resolution (1064 nm Nd:Yag emission, 120 mW). Optical absorption spectra of pressed wafers were recorded with a Shimadzu spectrometer model UV-2450.

3. Results

3.1 Synthesis and characterization of core-shell nanoparticles with embedded wires and anchored $Ti^{IV}OCo^{II}$ or $ZrOCo^{II}$ light absorbers

According to our previous work, asymmetrically functionalized *p*-oligo(phenylene vinylene) molecules with 3 aryl units bearing a sulfonyl and a carboxyl group at the respective *para* positions of the terminal aryl groups (PV3) cast into a 2 nm silica shell afford transport of positive charge (holes) upon injection from established organometallic visible light sensitizer to a Co_3O_4 core.[9-11,13] In order to elucidate charge transfer from all-inorganic heterobinuclear MMCT light absorbers to the Co oxide catalyst via silica embedded wire molecules by transient optical spectroscopy, separate monitoring of individual transfer steps, from binuclear unit to

embedded wire molecule and from wire to Co oxide core, is required. We selected MMCT units with a group IVB Ti or Zr acceptor and a late transition metal Co^{II} donor center because $Zr^{IV}OCo^{II}$ has been shown to drive water oxidation when coupled to a metal oxide nanocluster catalyst on the donor side while at the same time splitting CO_2 to CO at transient Zr center upon $Zr^{IV}OCo^{II} \rightarrow Zr^{III}OCo^{III}$ excitation.[1] Hence, the photo-excited ZrOCo unit is expected to activate the Co_3O_4 catalyst core while at the same time reduce CO_2. Since the focus of this work is on charge transfer between the binuclear light absorber and the molecular wire on the Co side, the majority of experiments were conducted with core-shell particles featuring the spectroscopically more straightforward TiOCo units.

According to our previous ultrafast study of hole transfer from a porphyrin light absorber to Co_3O_4 across an ultrathin silica layer with embedded PV3 wires, the charge arrives on the Co oxide catalyst core within 255 ps.[10] To prolong the lifetime of the hole on the embedded wire molecules by avoiding this ultrafast transfer step, the Co oxide core was replaced by SiO_2 which, as an insulator, cannot accept charge. The resulting SiO_2/TMSA-PV3/SiO_2/$Ti^{IV}OCo^{II}$ core-shell nanoparticles are suitable for the separate monitoring of the primary hole transfer step from excited binuclear light absorber to embedded PV3 molecule by transient optical absorption spectroscopy.

3.1.1 SiO_2/TMSA-PV3/SiO_2 core-shell nanoparticles

In order to achieve the required precision for selecting the concentration of covalently anchored PV3 molecules on the silica nanoparticle surface and broaden the tuning range compared to previously used methods, a new synthetic method was introduced. Up to now, anchoring of PV3 molecules was based on forming an ester linkage of a terminal carboxy group of PV3 with

surface silanol groups, or tripodal anchoring of PV3 by a terminal $(HOCH_2)_3C$ 'spider' group in a single step, which resulted in poor control of surface loading.[12] The new approach, illustrated in the top part of Scheme 1, consists of two separate steps, namely covalent surface attachment of a tripodal anchor followed by linking of PV3 through formation of an amide bond between anchor and the wire molecule. Two different tripodal anchors were used, namely 4-(trimethoxysilyl)aniline (TMSA) and tris(bromomethyl)-aminomethane hydrobromide (TBAM). TMSA reacts with the silica surface by silanation, while TBAM forms three spider-like C-O-Si bridges by nucleophilic substitution of Br by surface O at the methylene carbon.[18] In a subsequent step, amide linkage between the NH_2 group of anchored TMSA and the carboxyl moiety of the PV3 molecule, catalyzed by HATU, results in covalent wire attachment. For casting of the wire molecules into 2 nm of silica, a modified Stoeber method described previously was used.[11]

The core-shell nanoparticles were characterized by FT-IR, FT-Raman and UV-vis spectroscopy at each step of the assembly procedure. The FT-IR spectrum of a pressed pellet of powder of SiO_2 nanoparticles (12 nm) with anchored TMSA, Figure 1A trace (a), shows the NH_2 scissor deformation mode at 1626 cm^{-1} and the quadrant and semicircle stretching modes of the aromatic ring at 1604, 1512 and 1417 cm^{-1} (the weak 1489 and 1433 cm^{-1} bands are due to a small amount of *meta* functionalized anchor species). Aryl CH stretch modes are detected at 3058 and 3030 cm^{-1} (Figure S2).[19] Monitoring of the C-H stretching region allows to directly follow the anchoring of TMSA on silica by the disappearance of the 2956 to 2854 cm^{-1} modes of its methoxy groups, as shown for a partially anchored sample in Figure S2 by the red trace (a). The disappearance of these bands demonstrates complete tripodal anchoring upon hydrolysis of all methoxy groups in aqueous particle suspension at 100 ˚C (Figure S2 black trace (b)). While some

cross-linking of silyl aniline through horizontal oligomerization on the particle surface [20] cannot be ruled out, the sharp NH_2 band at 1626 cm^{-1} suggests that only a minor fraction, if any, of the anchor molecules oligomerize because the expected H bonding between NH_2 groups of adjacent units that would give rise to a broad absorption band is not observed.

The loading of TMSA anchor shown in Figure 1A was determined by UV spectroscopy. The absorption maxima for TMSA anchored on silica in aqueous suspension are at 202 nm, 245 nm ($S_0 \rightarrow S_2$, S_3) and 285 nm ($S_0 \rightarrow S_1$).[21] With $\varepsilon_{245} = 13{,}400\ L\ mol^{-1}\ cm^{-1}$ for TMSA in aqueous environment (see Figure S3) we estimate anchor loading of 0.3 TMSA nm^{-2} (see SI for details of calculation).[22]

Attachment of PV3 wire molecules to silica-anchored TMSA by reaction of the terminal carboxy group of the wire molecule with the anchor amine group is indicated by new amide vibrational modes at 1651 cm^{-1} (C=O stretch) and 1558 cm^{-1} (CNH bend, very weak) (Figure 1A, red trace (b)). Aryl ring modes at 1598 and 1515 cm^{-1} are superimposed by TMSA bands, while a new absorption at 1393 cm^{-1} originates from PV3 semicircle stretching mode of the aromatic ring. [23-27] The modes of anchored PV3 are more clearly seen after subtraction of the bands of unreacted TMSA anchors, as shown in Figure 1B, red trace (a), which was guided by the cancellation of the 1626 cm^{-1} NH_2 bend absorption of unlinked TMSA. Infrared spectra recorded after casting of the wires into 2 nm of silica remain unchanged (Figure 1 A, blue trace (c) and 1B, blue trace (b), the latter after subtracting unlinked TMSA bands), indicating structural integrity of the wire PV3 molecules despite the harsh (alkaline) conditions of the casting process.

While the infrared aromatic stretch modes of PV3 have relatively low intensity compared to the corresponding TMSA modes, the inverse holds for FT-Raman spectra as shown in Figure 2. Only the 1600 cm^{-1} aromatic stretch can be seen in the Raman spectrum of TMSA anchor as a

very weak band, trace (a), while the PV3 bands of the solid powder of wire molecules (trace (b), black) and PV3 anchored by TMSA on SiO_2 nanoparticles (trace (c), red) are much more intense. This allowed more accurate assessment of any structural changes of the molecular wire upon anchoring and after casting into silica. In agreement with the FT-IR result, of the five Raman modes of PV3 solid powder observed in the 1200 – 1700 cm^{-1} region at 1175, 1190, 1558, 1591, and 1631 cm^{-1},[23-27] all but the 1591 cm^{-1} aryl stretch mode remain at the same frequency upon anchoring on silica and subsequent casting into a silica nanolayer. This observation confirms that the structure of the wire molecule, in particular the all-trans configuration of the aryl moieties is not significantly influenced by anchoring and silica embedding. Specifically, the C=C stretch mode of PV3 at 1631 cm^{-1}, which is known to undergo large shifts for even modest out-of-plane distortions,[24,27,28] does not exhibit any change. In addition, the relative intensity of the 1631 cm^{-1} band with respect to the 1591 cm^{-1} mode reveals information about the effective conjugation length. Since there are also no changes observed in this regard, attachment of the molecular wire to the aromatic anchor via amidation does not increase the conjugation length, which is further supported by the absence of a substantial shift of the UV-vis absorption band. Nevertheless, the small blue shift of the 1591 cm^{-1} aryl stretch upon attachment to the silica surface, Figure 2 trace (c), manifests interaction with silica. The spectroscopic effect can more clearly be seen upon deconvolution shown in the expanded FT-Raman spectra of Figure 3. Figures 3a-d present spectra of the samples shown in Figure 2b-e, now on an expanded scale. Spectral deconvolution is adequately described by two components, namely the 1591 band of PV3 crystals of Figure 3a and the blue component with a peak at 1600 cm^{-1} that emerges upon anchoring on silica (Figure 3b). This new component, which signals interaction with silica, is rendered considerably more intense at the expense of the red component when applying high pressure during pressing of the

pellet for increasing the interaction with anchored wire molecules and silica surfaces of adjacent particles. When casting the wire molecules into the silica nanomembrane, only the blue component is observed (Figure 3d), consistent with complete encasing of the molecule while preserving its structure.

A small but significant effect of silica embedding of PV3 is also manifested in the optical spectra. UV-vis spectra of DMF solutions of PV3 (λ_{max} = 368 nm), PV3 covalently attached to silica nanoparticles (SiO_2/TMSA-PV3, λ_{max} = 372 nm), and embedded into a silica shell (SiO_2/TMSA-PV3/SiO_2, λ_{max} = 356 nm) in DMF suspension are shown in Figure 4. Taking the value of ε_{368} = 18,500 L mol^{-1} cm^{-1} for PV3 in DMF,[12] we estimate 0.8 % surface coverage of PV3, corresponding to a density of 0.02 nm^{-2}. Upon embedding the PV3 into the silica shell, the absorption maximum exhibits a modest blue shift of 12 nm to 354 nm. This is very close to the shift for a pressed pellet of SiO_2-TMSA-PV3 (Figure 4, dashed line), which indicates that the spectral shift manifests contact of the wire molecules with the silica environment.

3.1.2 Attachment of TiOCo or ZrOCo units

For anchoring of heterobinuclear TiOCo or ZrOCo light absorbers on the outer silica shell surface, the previously established synthetic method [17] needed to be modified in order to ensure the integrity of the silica embedded organic wire molecules during the assembly of the unit, as summarized in the bottom part of Scheme 1. Specifically, following tripodal anchoring of Ti centers using titanocene as precursor,[16] attachment of Co^{II} centers requires removal of the remaining cyclopentadienyl ligand on the Ti. However, calcination under aerated conditions at 550˚ C, successfully used before, would damage the PV3 molecules. Thus, a new mild approach based on photolytic dissociation was developed for removing the cyclopentadienyl ligand.

Excitation of the Ti^{IV}(cp) LMCT transition with a maximum at 325 nm, shown in Figure 5A trace (a), with 405 nm laser light results in photodissociation, most probably by homolytic cleavage of the Ti-cp π bond. Ti^{III} and cp• radical so formed subsequently react with the solvent by abstracting H from dichloromethane or ethanol.[29-31] ($CHCl_2$ or CH_3CH_2O radical, respectively, may attach to Ti^{III}, preventing re-coordination of cyclopentadienyl moieties).[31] As shown in Figure 5A, trace (b), the optical absorption disappeared completely after min 45 irradiation (170 mW). Further confirmation of removal of the cp ligand was obtained by infrared monitoring. The C-H stretching modes of the cp ring can be seen at 2978 and 2876 cm^{-1} and in the C-C stretch and CH bending region at 1475, 1392, and 1368 cm^{-1} (Figure 5B, trace (a)). These bands vanish almost completely upon photolysis (Figure 5B, trace (b)). From the loss of C-H stretch absorption of cp at 2978 cm^{-1}, we estimate a lower limit of photolytic detachment of cp from Ti^{iV} of 94%. New absorptions emerge in the C-H stretch and fingerprint regions, including what is likely a C=O mode at 1650 cm^{-1} (Figure 5B, trace (b)). The C-H stretch modes at 2928, 2856 and the bend absorption at 1450 cm^{-1} (broad) are typical of methoxy and ethoxy moieties, likely originating from cp• radicals that have reacted with the surrounding solvent. For the assembly of ZrOCo, the same synthetic protocol was used except that for photoelimination of cp ligand, the UV emission of a Xe arc lamp was used because the Zr^{IV}(cp) LMCT is located at wavelengths shorter than 400 nm.

The new mild synthetic method affords TiOCo functionalized core-shell nanoparticles with intact silica embedded PV3 wire molecules, as evidence by the optical spectra of Figure 6. Figure 6A trace (a) of SiO_2/TMSA-PV3/SiO_2-Ti particles features the UV band of embedded PV3 (maxima at 356 and 339 nm), and the onset of the Ti-O LMCT band at 330 nm, but no absorption of cp or any other species. Upon attachment of Co centers for obtaining the TiOCo

unit, the continuous tail of the $Ti^{IV}OCo^{II} \rightarrow Ti^{III}OCo^{III}$ transition appears, with onset between 600 and 700 nm increasing monotonously towards the UV, as shown in Figure 6B trace (b). The MMCT absorption is superimposed by the characteristic Co^{II} d-d bands in the 550-700 nm region. Infrared spectra of the same samples presented in Figure 7A feature TMSA-PV3 bands, which for Ti (trace (b)) and TiOCo (trace (c) functionalized particles contain residual alkyl groups shown in Figure 5B, trace (b). Corresponding FT-Raman spectra (Figure 7B) exhibit exclusively the bands of embedded molecular wires and the impurity band at 1454 cm^{-1} already noted in the infrared spectrum.

Alternatively, our new method of using Tetrakis(diethylamido)titanium(IV) as precursor for tripodal anchoring of Ti centers resulted in SiO_2/TMSA-PV3/SiO_2-TiOCo nanoparticles showing the same UV-vis absorptions (Figure S3) as obtained for samples prepared by the titanocene approach (Figure 6). Hence, this approach provides fully functionalized nanoparticles with intact embedded PV3 wire molecules as well.

3.2 Hole transfer from TiOCo unit to PV3 molecules

To explore hole transfer from transient Co^{III} generated by MMCT excitation of the $TiOCo^{II}$ light absorber to PV3 wires, we first performed nanosecond transient absorption measurements of silica nanoparticles with anchored $TiOCo^{II}$ and physisorbed sodium 2,2′-((1E,1′E)-1,4-phenylenebis(ethene-2,1-diyl))dibenzenesulfonate (abbrev. Na_2_PV3_$2SO_3$) on the particle surface. Loading of the silica surface with wire molecules and $[Co^{III}(NH_3)_5Cl]^{2+}$ sacrificial electron acceptor was performed by dispersing silica nanoparticles with anchored $TiOCo^{II}$ in aqueous solution of Na_2_PV3_$2SO_3$ and $[Co^{III}(NH_3)_5Cl]^{2+}Cl_2$, followed by removal of the solvent

by evacuation. The loaded nanoparticles were pressed into optically transparent wafers and held in argon atmosphere. Surface concentrations were estimated to be 0.7 nm^{-2} for TiOCo, 0.1 nm^{-2} for PV3, and 0.1 nm^{-2} for $[Co^{III}(NH_3)_5Cl]^{2+}$.

Excitation of the $Ti^{IV}OCo^{II}$ → $Ti^{III}OCo^{III}$ MMCT state of the light absorber with 8 ns laser pulses at 430 nm (10 mJ $pulse^{-1}$) resulted in a transient absorption in the 500 – 630 nm region with the maximum at 600 nm typical for $PV3^+$ radical cation [11,12,32] as shown in Figure 8 trace (a). The transient $PV3^+$ signal lasts for hundreds of μs. Concurrent electron transfer from transient Ti^{III} of the excited MMCT state to $[Co^{III}(NH_3)_5Cl]^{2+}$ acceptor is directly observed by the decrease of the infrared bands of NH_3 ligands as these are known to dissociate from the Co^{III} center upon reduction to Co^{II}.[33] The FT-IR difference spectrum before and after 15 min irradiation of the sample at 405 nm presented in Figure 9 shows the decrease of the characteristic 1615 and 1320 cm^{-1} bands of $[Co^{III}(NH_3)_5Cl]^{2+}$ along with the NH stretch at 3315 cm^{-1} under concurrently growth of free surface adsorbed NH_3 at 1611 and 3366 cm^{-1}. The absence of the transient $PV3^+$ spectrum under identical experimental conditions for the monometallic particles SiO_2-Ti^{IV} (Figure 8 trace (b)) and SiO_2-Co^{II} (trace (c)) confirms that hole transfer to the wire molecule is caused by excitation of the $TiOCo^{II}$ MMCT transition. SiO_2-TiOCo samples loaded with PV3 but without added $[Co^{III}(NH_3)_5Cl]^{2+}$ acceptor exhibit a small $PV3^+$ signal, indicating that some hole transfer from transient Co^{III} to PV3 does take place in competition with $Ti^{III}OCo^{III}$ → $Ti^{IV}OCo^{II}$ back electron transfer. The risetime of the $PV3^+$ absorption, shown in Figure 10a, is within the 8 ns duration of the 430 nm excitation pulse indicating hole transfer time from transient Co^{III} to PV3 of a few ns or less. The decay of the wire radical cation proceeds by a multi-exponential process over hundreds of μs, which is many orders of magnitude slower than the previously measured 255 ps when SiO_2 core is replaced by the Co_3O_4 catalyst.[10] While

charge recombination of $PV3^+$ radical cation with reduced donor is energetically favored (driving force +0.92V [33,34]), regeneration of $[Co^{III}(NH_3)_5Cl]^{2+}$ will not occur because the ligands dissociate irreversibly upon electron transfer. More likely, fragments of the dissociated complex are involved in re-reduction of $PV3^+$. The highly dispersive nature of the decay kinetics is consistent with the random distribution of physisorbed PV3 and acceptor species on the silica surface.

Of the two alternative preparations of SiO_2/TMSA-PV3/SiO_2 particles with anchored TiOCo light absorbers, infrared spectra of samples using $Ti(NEt_2)_4$ precursor method showed only residual diethylamine originating anchoring of the precursor (Figure S4C), but no unidentified impurity encountered with the titanocene method (Figure 7). Because it is an electron donor, any diethylamine, if participating in a charge transfer process, would diminish rather than enhance formation of PV3 radical cation. Therefore, we used $Ti(NEt_2)_4$ based SiO_2/TMSA-PV3/SiO_2-TiOCo nanoparticles to explore MMCT induced hole transfer from excited TiOCo light absorber to silica embedded PV3 molecules. As shown in Figure 10B, the 600 nm transient absorption of $PV3^+$ radical cation is observed with prompt (< 8 ns) rise upon excitation of TiOCo with a 430 nm laser pulse.

4. Discussion

The new two-step approach for anchoring the organic wire molecules upright on the oxide support provides a substantially more accurate method of selecting and tuning the loading level of the wire molecules than available in previous work. In particular, tripodal anchoring of the TMSA molecules can readily be verified by the disappearance of the infrared bands of methoxy

groups of the silane precursor. Furthermore, the well resolved, unaltered fingerprint FT-IR spectra of the attached anchor (Figure 1A) for loading up to 0.3 nm^{-2}, and comparison with spectra of free TMSA, indicate that surface aggregation of anchor molecules does not occur. This strongly suggests random distribution of TMSA anchors on the oxide surface. Subsequent attachment of PV3 wire molecules to anchored TMSA proceeds by catalyzed formation of amide linkages under mild room temperature conditions, which affords control of dosing and, hence, of the resulting wire density. Similarly, the sharp FT-Raman bands of attached wires observed both before and after silica casting indicates that aggregation on the surface is below the detection limit. While the loading levels used proved convenient for the spectroscopic studies reported here, results of photocatalytic efficiency evaluation of the complete core-shell assembly will guide the choice of embedded wire concentrations required for optimal performance.

The observed structural integrity of anchored wire molecule upon casting of amorphous silica enforces recent observations by other groups on organic (or organometallic) light absorbers or catalysts embedded in nanoscale oxide layers, mainly silica, alumina or titania using the atomic layer deposition technique (ALD). Organic dyes of dye-sensitized solar cells anchored on TiO_2 enshrouded in a nanoscale silica layer were found to retain their structural integrity and optical properties while exhibiting substantially improved performance.[35] Similarly, the widely used molecular chromophore perylene-3,4-dicarboximide anchored on a nickel oxide cathode was found by optical spectroscopy to be free of aggregation upon casting into 2 nm of alumina and shows drastically improved chemical stability in air and under light. Efficient visible light induced electron transfer to a hydrogen evolution catalyst in close proximity was reported.[36,37] The increased performance by alumina casting is attributed to disaggregation and blocking of excimer formation of the light absorber molecules. At the same time, the ultrathin alumina

drastically stabilizes the chromophore by suppressing desorption from the oxide surface. These advantages were also found upon alumina casting of Ru based organometallic chromophores and water oxidation catalysts on TiO_2 anode.[38,39]

Hole transfer from transient $Ti^{III}OCo^{III}$ generated by $Ti^{IV}OCo^{II} \rightarrow Ti^{III}OCo^{III}$ excitation benefits from the rectifying electronic property of the TiOCo PV3 assembly. As shown in Scheme 2, transient Ti^{III} does not possess sufficient reducing potential for electron transfer to the LUMO of PV3 while the potential of transient Co^{III} donor center is well aligned for hole transfer to the HOMO of the wire molecule.[12,34] Therefore, TiOCo excited to the MMCT state is poised to transfer an electron to an acceptor, which is pentamine chloro cobalt for experiments presented here, or a Cu nanoparticle catalyst for CO_2 reduction reported in previous work [3] (the TiOCo MMCT-induced overall charge transfer process leading to wire radical cation and reduced acceptor is endoergic by 1 V (Scheme 2)). Hence, the HOMO and LUMO potentials of the wire relative to the excited MMCT redox potential are directing hole transfer to the wire molecule while preventing undesired electron injection into PV3. This electronic property of PV3 is critical for enabling visible light induced hole transfer to wire molecules in nanometer distance without the need for spatial organization e.g. by molecularly defined linkage between the Co donor center of the TiOCo light absorber and PV3.

5. Conclusions

Introduction of a new synthetic approach that consists of surface attachment of a tripodal anchor followed by linking to a wire molecule has enabled accurate selection of the loading level and ease of tuning of the surface concentration of wires embedded in an ultrathin silica separation

membrane. Infrared, Raman and optical spectroscopy revealed that surface attachment of the PV3 molecules and casting into amorphous silica does not result in structural changes of the wire molecules. At the same time, spectral signature of the interaction of PV3 with the silica environment was uncovered by FT-Raman and optical spectroscopy.

Hole transfer from visible light excited $Ti^{IV}OCo^{II} \rightarrow Ti^{III}OCo^{III}$ chromophore anchored on the silica shell surface to embedded wire molecules is manifested by transient optical absorption of the wire radical cation with a maximum at 600 nm. The rise of the band occurs within the width of the laser excitation pulse, indicating charge transfer within a few ns or faster. The flexible choice of redox potentials of heterobinuclear unit and PV3 allows to impart rectifying property on the light absorber-wire assembly, which relaxes the need for developing a molecularly defined linkage. As shown in previous work, when the wires are anchored on Co_3O_4 catalyst surface, hole injection from silica embedded wire into the water oxidation catalyst proceeds on the ultrafast time scale.[10] Therefore, combined with the result reported here, hole transfer from excited TiOCo light absorber across the silica membrane via embedded PV3 wires proceeds within 8 ns or faster.

Together with the recently reported visible light driven electron transfer from the group IV acceptor center of excited TiOCo or ZrOCo units to cuprous oxide nanocluster catalyst for CO_2 reduction,[3] concurrent hole transfer from the Co donor center across the silica membrane to Co oxide catalyst for water oxidation revealed by this work opens up exploration of complete photosynthetic cycles using nanoscale core-shell architecture.

Supporting Information

Calculation of surface coverage of anchors and molecular wires, FT-IR and UV-vis spectra at various stages of assembly.

Acknowledgment

This work was supported by the Director, Office of Science, Office of Basic Energy Sciences, Division of Chemical, Geological and Biosciences of the U.S. Department of Energy under Contract No. DE-AC02-05CH11231. G.K. gratefully acknowledges the scholarship support from the German Research Foundation (DFG, agreement KA 4403/1-1).

References

[1] Kim, W.; Yuan, G.; McClure, B. A.; Frei, H. Light Induced Carbon Dioxide Reduction by Water at Binuclear $ZrOCo^{II}$ Unit Coupled to Ir Oxide Nanocluster Catalyst. *J. Am. Chem. Soc.* **2014**, *136*, 11034-11042.

[2] Han, H.; Frei, H. In Situ Spectroscopy of Water Oxidation at Ir Oxide Nanocluster Driven by Visible TiOCr Charge-Transfer Chromophore in Mesoporous Silica. *J. Phys. Chem. C* **2008**, *112*, 16156-16159.

[3] Kim. W.; Frei, H. Directed Assembly of Cuprous Oxide Nanocatalyst for CO_2 Reduction Coupled to Heterobinuclear $ZrOCo^{II}$ Light Absorber in Mesoporous Silica. *ACS Catal.* **2015**, *5*, 5627-5635.

[4] Kim, W.; Edri, E.; Frei, H. Hierarchical Inorganic Assemblies for Artificial Photosynthesis. *Acc. Chem. Res.* **2016**, *49*, 1634-1645.

[5] Kim, W.; McClure, B. A.; Edri, E.; Frei, H. Coupling of Carbon Dioxide Reduction with Water Oxidation in Nanoscale Photocatalytic Assemblies. *Chem. Soc. Rev.* **2016**, *45*, 3221-3243.

[6] Nakamura, R.; Okamoto, A.; Osawa, H.; Irie, H.; Hashimoto, K. Design of All-Inorganic Molecular-Based Photocatalysts Sensitive to Visible Light: Ti(IV)-O-Ce(III) Bimetallic Assemblies on Mesoporous Silica. *J. Am. Chem. Soc.* **2007**, *129*, 9596-9597.

[7] Okamoto, A.; Nakamura, R.; Osawa, H.; Hashimoto, K. Site-Specific Synthesis of Oxo-Bridged Mixed-Valence Binuclear Complexes on Mesoporous Silica. *Langmuir* **2008**, *24*, 7011-7017.

[8] Edri, E.; Aloni, S.; Frei, H. Fabrication of Core-Shell Nanotube Array for Artificial Photosynthesis Featuring an Ultrathin Composite Separation Membrane. *ACS Nano* **2018**, *12*, 533-541.

[9] Edri, E.; Frei, H. Charge Transport through Organic Molecular Wires Embedded in Ultrathin Insulating Inorganic Layer. *J. Phys. Chem. C* **2015**, *119*, 28326-28334.

[10] Edri, E.; Cooper, J. K.; Sharp, I. D.; Guldi, D. M.; Frei, H. Ultrafast Charge Transfer between Light Absorber and Co_3O_4 Water Oxidation Catalyst across Molecular Wires Embedded in Silica Membrane. *J. Am. Chem. Soc.* **2017**, *139*, 5458-546.

[11] Agiral, A.; Soo, H. S.; Frei, H. Visible Light Induced Hole Transport from Sensitizer to Co_3O_4 Water Oxidation Catalyst across Nanoscale Silica Barrier with Embedded Molecular Wires. *Chem. Mater.* **2013**, *25*, 2264-2273.

[12] Soo, H. S.; Agiral, A.; Bachmeier, A.; Frei, H. Visible Light-Induced Hole Injection into Rectifying Molecular Wires Anchored on Co_3O_4 and SiO_2 Nanoparticles. *J. Am. Chem. Soc.* **2012**, *134*, 17104-17116.

[13] Yuan, G.; Agiral, A.; Pellet, N.; Kim. W.; Frei, H. Inorganic Core-Shell Assemblies for Closing the Artificial Photosynthetic Cycle. *Faraday Discuss.* **2014**, *176*, 233-249.

[14] Cornejo, J. A.; Sheng, H.; Edri, E.; Ajo-Franklin, C. M; Frei, H. Nanoscale Membranes that Chemically Isolate and Electronically Wire Up the Abiotic/Biotic Interface. *Nature Commun.* **2018**, *9*: 2263.

[15] Marchand, A. P.; Rajagopal, D.; Bott, S. G.; Archibald, T. G. A Novel Approach to the Synthesis of 1,3,3-trinitroazetidine. *J. Org. Chem.* **1995**, *60*, 4943-4946.

[16] Maschmeyer, T.; Rey, F.; Sankar, G.; Thomas, J. M. Heterogeneous Catalysts Obtained by Grafting Metallocene Complexes onto Mesoporous Silica. *Nature* **1995**, *378*, 159-162.

[17] Han, H.; Frei, H. Visible Light Absorption of Binuclear $TiOCo^{II}$ Charge-Transfer Unit Assembled in Mesoporous Silica. *Microporous Mesoporous Mater.* **2007**, *103*, 265-272.

[18] Banet, P.; Marcotte, N.; Lerner, D. A.; Brunel, D. Single-Step Dispersion of Functionalities on a Silica Surface. *Langmuir* **2008**, *24*, 9030-9037.

[19] Bellamy, L. J. *The Infrared Spectra of Complex Molecules,* 3rd ed.; Chapman and Hall: London, Vol. 1, 1975. p 73.

[20] Acres, R. G.; Ellis, A. V.; Alvino, J.; Lenahan, C. E.; Khodakov, D. A.; Metha, G. F.; Andersson, G. G. Molecular Structure of 3-Aminopropyltriethoxysilane Layers Formed on Silanol-Terminated Silicon Surfaces. *J. Phys. Chem. C* **2012**, *116*, 6289-6297.

[21] Cumper, C. W. N.; Singleton, A., The ultraviolet spectra of aniline, 2-, 3-, and 4-aminopyridines and of some of their derivatives in n-hexane, 1,4-dioxane, ethanol, and water solutions. *J. Chem. Soc. B* **1968**, 649-651.

[22] Zhuravlev, L. T. The Surface Chemistry of Amorphous Silica. Zhuravlev model. *Colloids Surf. A: Physicochem. Eng. Aspects* **2000**, *173*, 1-38.

[23] Piacenza, M.; Comoretto, D.; Burger, M.; Morandi, V.; Marabelli, F.; Martinelli, C.; Farinola, G. M.; Cardone, A.; Gigli, G.; Della Sala, F. Raman Spectra of Poly(p-phenylenevinylene)s with Fluorinated Vinylene Units: Evidence of Inter-ring Distortion. *ChemPhysChem* **2009**, *10*, 1284-1290.

[24] Tian, B.; Zerbi, G.; Schenk, R.; Müllen, K. Optical Spectra and Structure of Oligomeric Models of Polyparaphenylenevinylene. *J. Chem. Phys.* **1991**, *95*, 3191-3197.

[25] Tian, B.; Zerbi, G.; Müllen, K. Electronic and Structural Properties of Polyparaphenylenevinylene from the Vibrational Spectra. *J. Chem. Phys.* **1991**, *95*, 3198-3207.

[26] Hrenar, T.; Mitrić, R.; Meić, Z.; Meier, H.; Stalmach, U. Vibrational Spectra and DFT Calculations of PPV-oligomers. *J. Mol. Struct.* **2003**, *661*, 33-40.

[27] Burrezo, P. M.; Zhu, X.; Zhu, S.-F.; Yan, Q.; López Navarrete, J. T.; Tsuji, H.; Nakamura, E.; Casado, J. Planarization, Fusion, and Strain of Carbon-Bridged Phenylenevinylene Oligomers Enhance π-Electron and Charge Conjugation: A Dissectional Vibrational Raman Study. *J. Am. Chem. Soc.* **2015**, *137*, 3834-3843.

[28] Bellamy, L. J. *The Infrared Spectra of Complex Molecules.* 3rd ed.; Chapman and Hall: London, Vol. 1, 1975. p 37.

[29] Van Tamelen, E. E.; Brauman, J. I.; Ellis, L. E. Photolysis of Cyclopentadienide and Cyclopentadiene. *J. Am. Chem. Soc.* **1971**, *93*, 6145-6151.

[30] Harrigan, R. W.; Hammond, G. S.; Gray, H. B. Photochemistry of titanocene(IV) derivatives. *J. Org. Chem.* **1974**, *81*, 79-85.

[31] Tsai, Z.-T.; Brubaker, C. H. Photolysis of Titanocene Dichloride. *J. Organomet. Chem.* **1979**, *166*, 199-210.

[32] Deussen, M.; Bassler, H. Anion and Cation Absorption Spectra of Conjugated Oligomers and Polymers. *Chem. Phys.* **1992**, *164*, 247-257.

[33] Curtis, N. J.; Lawrance, G. A.; Sargeson, A. M. Reduction Potentials of Pentammine Complexes of Cobalt(III), Rhodium(III), and Iridium(III): Physical Correlations. *Aust. J. Chem.* **1983**, *36*, 1327-1339.

[34] Davis, W. B.; Ratner, M. A.; Wasielewski, M. R. Dependence of Electron Transfer Dynamics in Wire-Like Bridge Molecules on Donor-Bridge Energetics and Electronic Interactions. *Chem. Phys.* **2002**, *281*, 333.

[35] Son, H. J.; Wang, X.; Prasittichai, C.; Jeong, N. C.; Aaltonen, T.; Gordon, R. G.; Hupp, J. T. Glass-Encapsulated Light Harversters: More Efficient Dye-Sensitized Solar Cells by Deposition of Self-Aligned, Conformal, and Self-Limited Silica Layers. *J. Am. Chem. Soc.* **2012**, *134*, 9537-9540.

[36] Kamire, R. J.; Majewski, M. B; Hoffeditz, W. L.; Phelan, B. T.; Farha, O. K.; Hupp, J. T.; Wasielewski, M. R. Photodriven Hydrogen Evolution by Molecular Catalysts Using Al_2O_3-Protected Perylene-3,4-Dicarboximide on NiO Electrodes. *Chem. Sci.* **2017**, *8*, 541-549.

[37] Kamire, R.J.; Materna, K. L.; Hoffeditz, W. L.; Phelan, B. T.; Thomsen, J. M.; Farha, O. K.; Hupp, J. T.; Brudvig, G. W.; Wasielewski, M. R. Photodriven Oxidation of Surface-Bound Iridium-Based Molecular Water-Oxidation Catalysts on Perylene-3,4-dicarboximide-Sensitized TiO_2 Electrodes Protected by an Al_2O_3 Layer. *J. Phys. Chem. C* **2017**, *121*, 3752-3764.

[38] Lapides, A. M.; Sherman, B. D.; Brennaman, M. K.; Dares, C. J.; Skinner, K. R.; Templeton, J. L.; Meyer, T. J. Synthesis, Characterization, and Water Oxidation by a Molecular Chromophore-Catalyst Assembly Prepared by Atomic Layer Deposition. The "Mummy" Strategy. *Chem. Sci.* **2015**, *6*, 6398-6406.

[39] Vannucci, A. K.; Alibabaei, L.; Losego, M. D.; Concepcion, J. J.; Kalanyan, B.; Parson, G. N.; Meyer, T. J. Crossing the Divide between Homogeneous and Heterogeneous Catalysis in Water Oxidation. *Proc. Natl. Acad. Sci. USA* **2013**, *110*, 20918-20922.

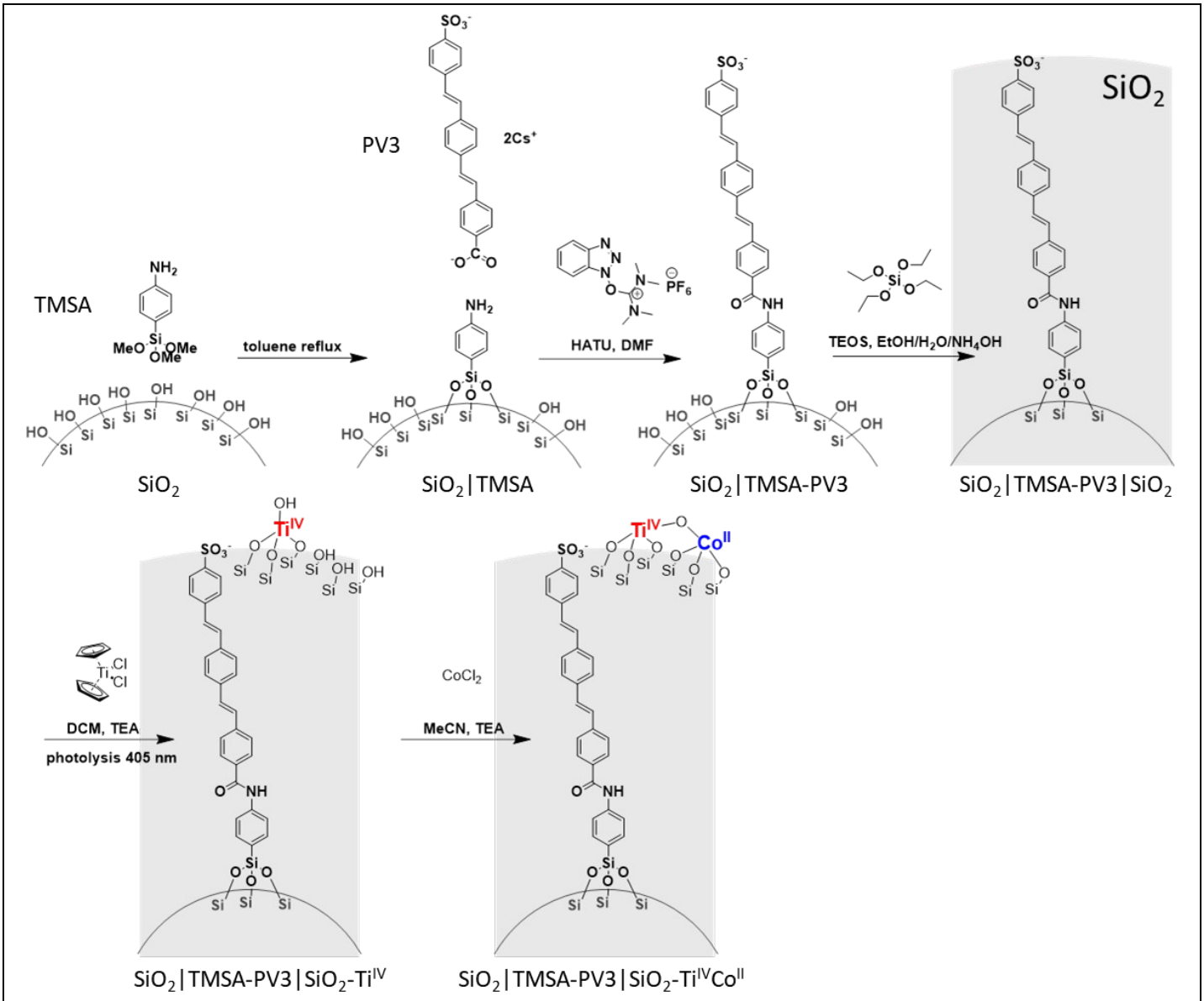

Scheme 1: Assembly of PV3 wires vertically aligned on silica nanoparticles cast into an ultrathin silica layer, surface attachment of Ti^{IV}-O-Co^{II} light absorber.

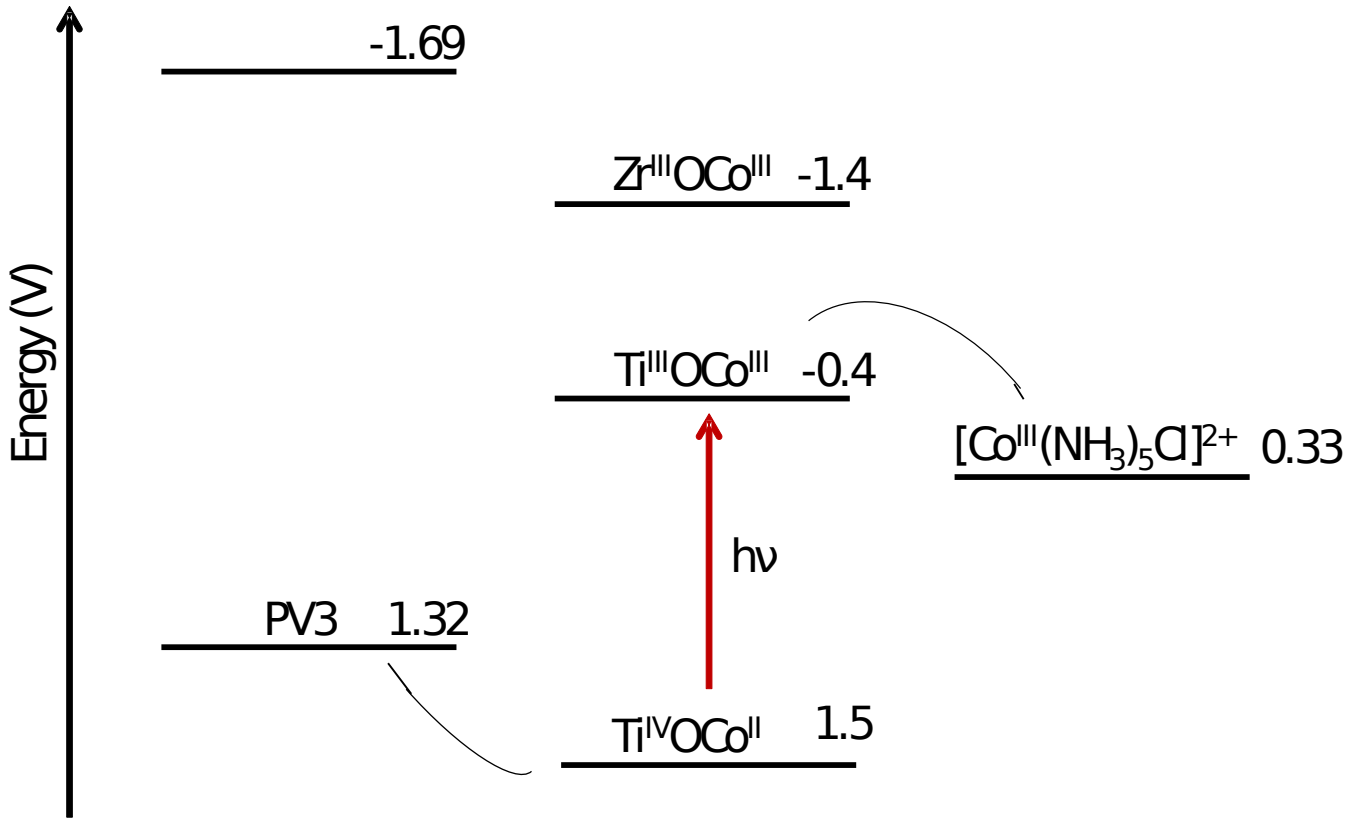

Scheme 2: Energy diagram of electronic states involved in the observed charge transfer processes of the SiO_2/TMSA-PV3/SiO_2-$TiOCo^{II}$ system. Estimated potentials according to literature reports.[33,34]

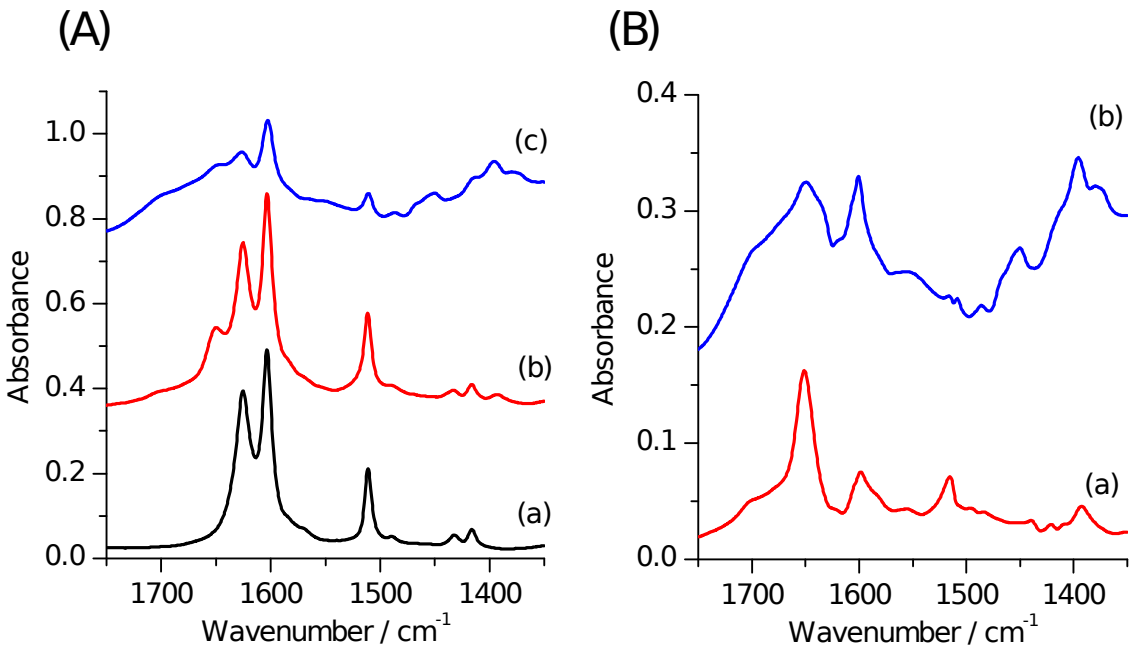

Figure 1: FT-IR spectra of pressed wafers of functionalized SiO_2 nanoparticles. A) Trace (a) shows FT-IR spectrum of SiO_2/TMSA (black). Trace (b) SiO_2/TMSA-PV3 (red). Trace (c) SiO_2/TMSA-PV3/SiO_2 (blue). SiO_2 was taken as background. B) Trace (a) FT-IR spectra of SiO_2/TMSA-PV3 (red) and trace (b) SiO_2/TMSA-PV3/SiO_2 (blue) showing only PV3 modes after subtracting bands of free TMSA. Very small peaks at 1486 and 1450 cm^{-1} are due to residual ethoxy moieties of the silica precursor.

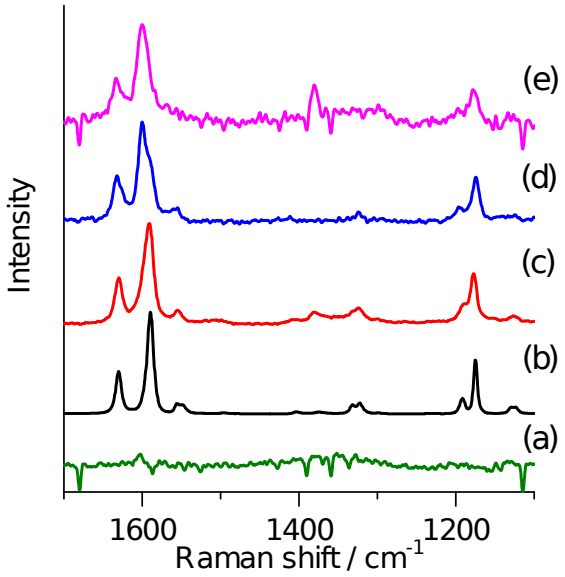

Figure 2: FT-Raman spectra of powders of (a) SiO_2/TMSA (green). (b) PV3 crystallites (black). (c) SiO_2/TMSA-PV3 (red). (d) SiO_2/TMSA-PV3 pressed into a pellet at 10 ton (blue). (e) SiO_2/TMSA-PV3/SiO_2 (pink).

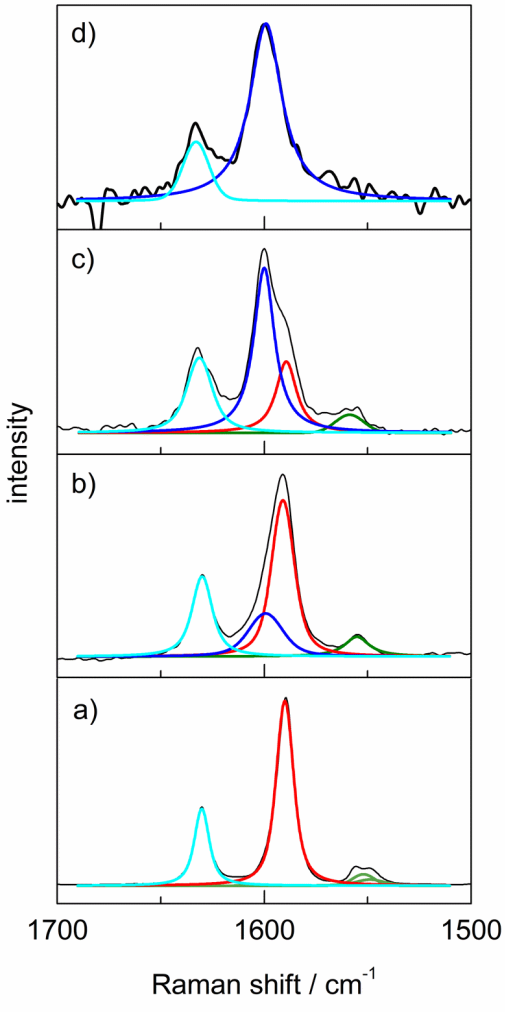

Figure 3: FT-Raman spectra of a) PV3 crystal powder. b) SiO_2/TMSA-PV3. c) SiO_2/TMSA-PV3 pressed pellet (10 ton). d) SiO_2/TMSA-PV3/SiO_2. Deconvolution by Voigt fit function shown. The red Voigt profile is the Raman band for plain PV3, while the dark blue Voigt profile corresponds to PV3 molecules interacting with surrounding silica.

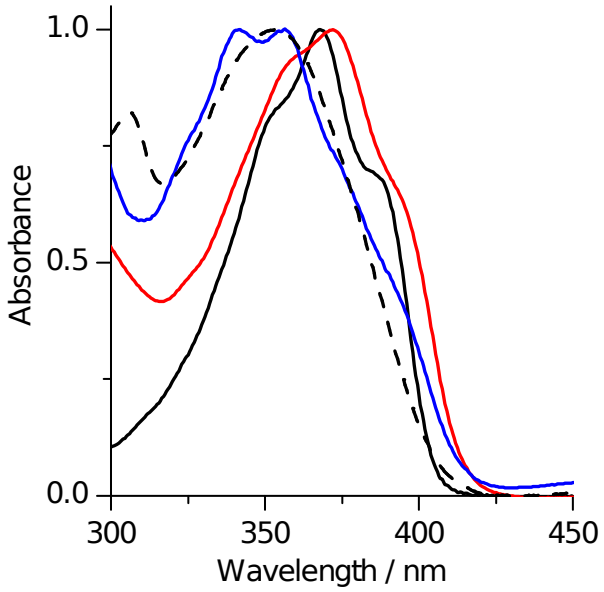

Figure 4: Normalized absorption spectra of DMF solutions of pure PV3 (black), SiO_2/TMSA-PV3 (red), and SiO_2/TMSA-PV3/SiO_2 (blue). The dashed trace (black) is a pressed pellet of SiO_2/TMSA-PV3 held in vacuum (absorbance contribution due to light scattering subtracted).

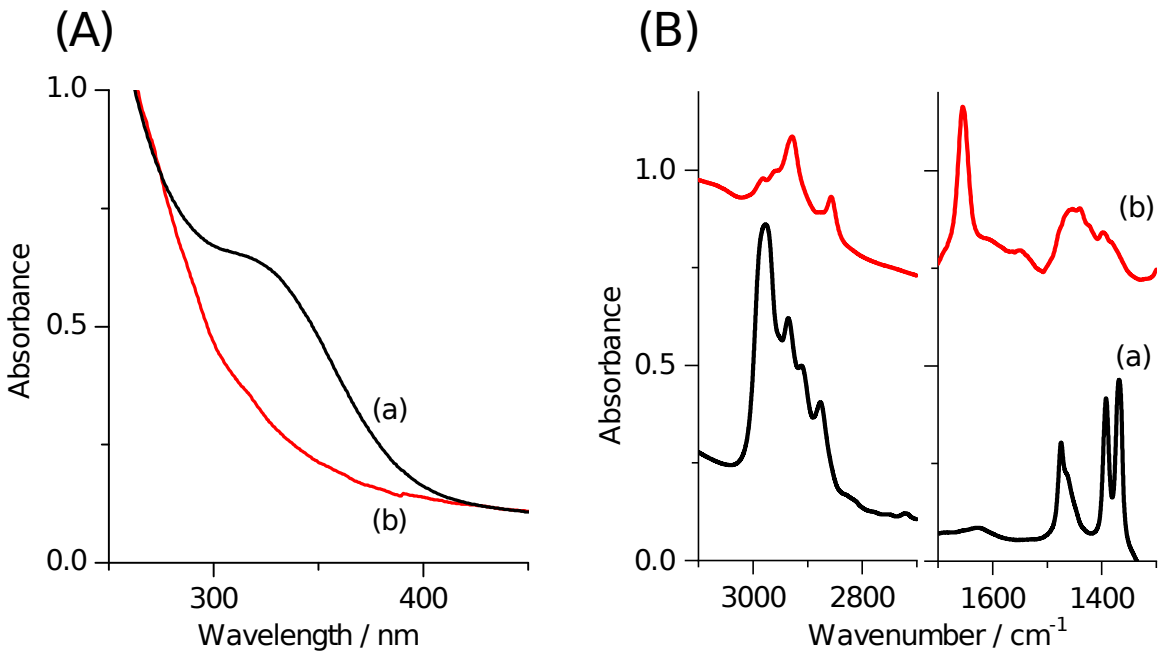

Figure 5: (A) UV-vis absorption spectrum of SiO_2-Ti^{IV}cp (black trace (a)) and resulting photolyzed SiO_2-Ti^{IV} (red trace (b)) in dichloromethane suspension (scattering contribution to absorbance subtracted, c = 2.5 mg/mL). Photolysis time is 45 min at 170 mW. (B) FT-IR spectra of same samples.

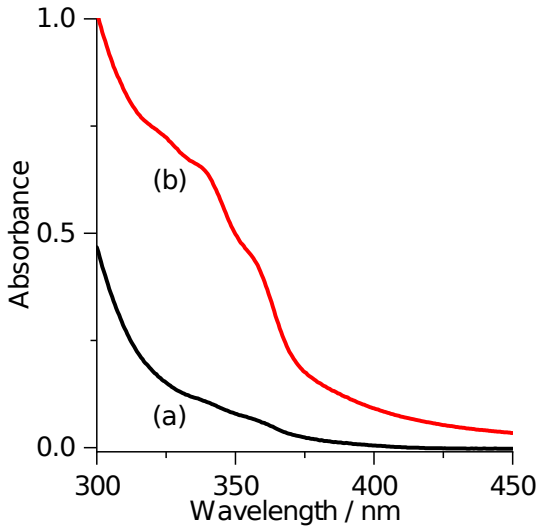

Figure 6: UV-vis absorption spectra of SiO_2/TMSA-PV3/SiO_2-Ti^{IV} in DMF suspension (trace (a), black) and SiO_2/TMSA-PV3/SiO_2-$Ti^{IV}OCo^{II}$ (trace (b), red) in DMF suspension (scattering contribution to absorbance subtracted, concentration 2.5 mg mL^{-1}). Sample (b) is sample (a) after the anchoring of Co.

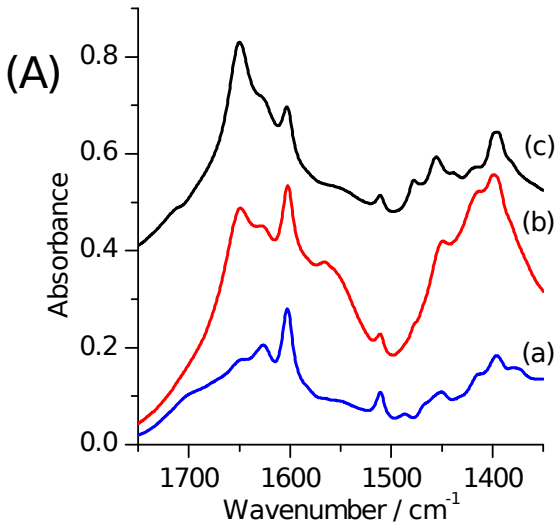

Figure 7: (A) (a) FT-IR of SiO_2/TMSA-PV3/SiO_2 (blue trace, repeated from Figure 1A(c)). (b) SiO_2/TMSA-PV3/SiO_2-Ti^{IV} (red trace). (c) SiO_2/TMSA-PV3/SiO_2-$Ti^{IV}OCo^{II}$ (black trace). (B) FT-Raman spectra of samples shown in panel (A).

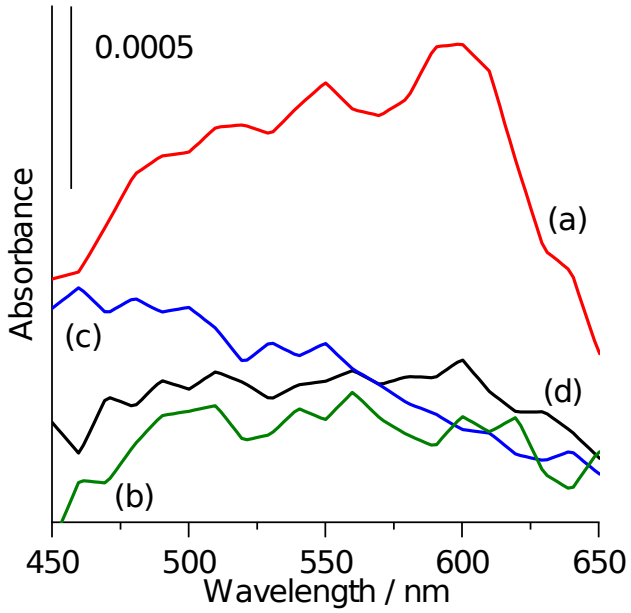

Figure 8: Nanosecond transient absorption spectra at 25 μs after 430 nm excitation of solid state transparent pressed pellet samples (a) SiO_2-TiOCo with physisorbed PV3 (0.1 nm^{-2}) and $[Co(NH_3)_5Cl]Cl_2$ (0.1 nm^{-2}); (b) SiO_2-Ti with physisorbed PV3 (0.1 nm^{-2}) and $[Co(NH_3)_5Cl]Cl_2$ (0.1 nm^{-2}); (c) SiO_2-Co with physisorbed PV3 (0.1 nm^{-2}) and $[Co(NH_3)_5Cl]Cl_2$ (0.1 nm^{-2}); (d) SiO_2-TiOCo with physisorbed PV3 (no $[Co(NH_3)_5Cl]Cl_2$). The spectra were corrected for electrostriction by subtracting the absorbance at 660 nm from the observed signal at each

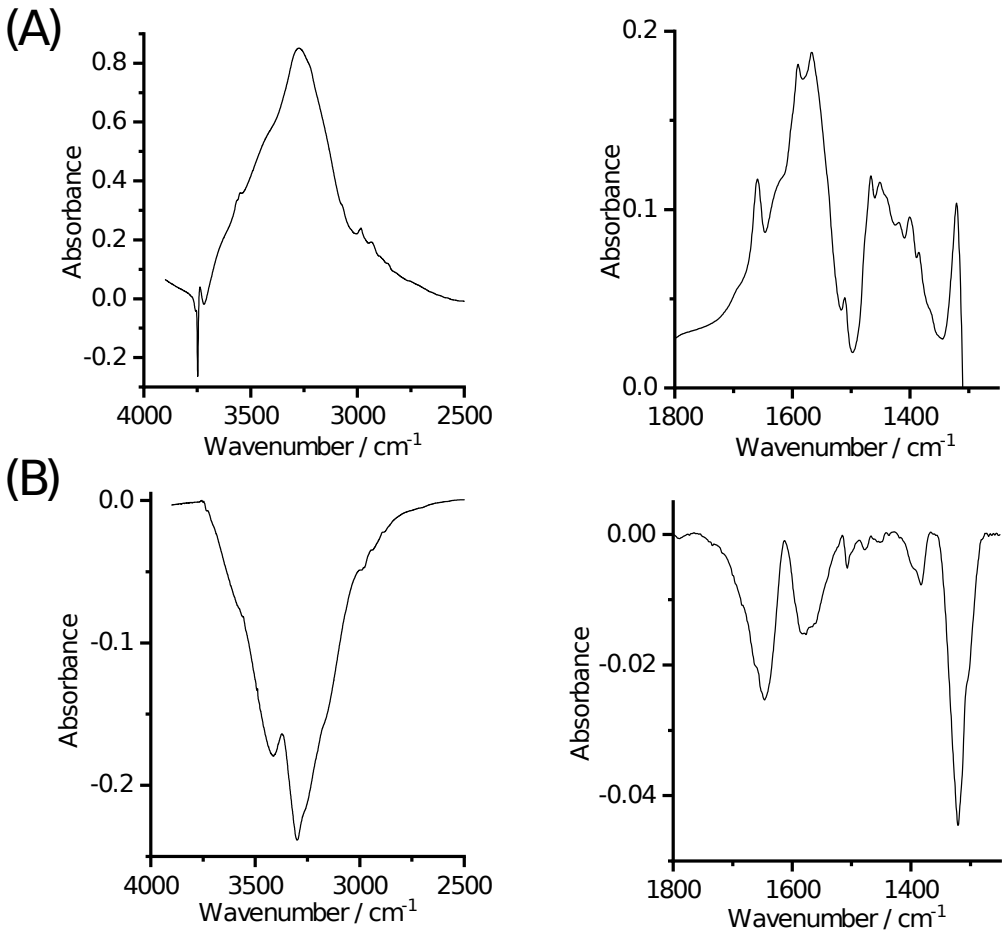

Figure 9: (A) FT-IR spectrum of SiO_2-TiOCo particles with physisorbed PV3 (0.1 nm^{-2}) and $[Co(NH_3)_5Cl]Cl_2$ (0.1 nm^{-2}) acceptor. SiO_2 background subtracted. (B) FT-IR difference spectrum after 15 min irradiation with 476 nm continuous laser emission showing depletion of $[Co(NH_3)_5Cl]^{2+}$ under growth of adsorbed ammonia.

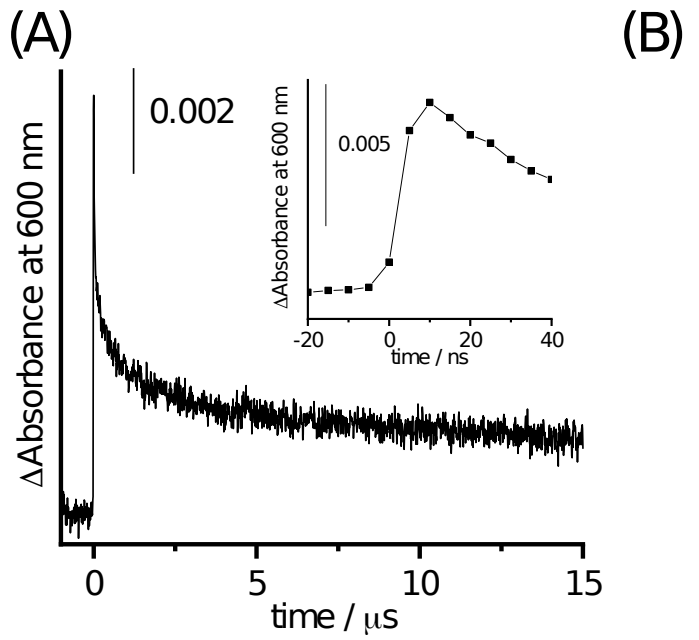

Figure 10: Kinetics of transient absorption of wire radical cation at 600 nm upon excitation at 430 nm with 8 ns pulse. (A) Pressed pellet of SiO_2-TiOCo silica nanoparticles with physisorbed PV3 (0.1 nm^{-2}) and $[Co(NH_3)_5Cl]Cl_2$ (0.1 nm^{-2}). The kinetic data show slow $PV3^{\bullet+}$ back electron transfer to ground state. Inset: expanded time axis showing laser pulse width limited rise. (B) Pressed pellet of SiO_2/TMSA-PV3/SiO_2-TiOCo with embedded PV3 (0.02 nm^{-2}) and $[Co(NH_3)_5Cl]Cl_2$ (0.1 nm^{-2}). The traces are corrected for the slow electrostriction signal by subtracting the SiO_2/TMSA-PV3/SiO_2-TiOCo trace (no $[Co(NH_3)_5Cl]Cl_2$ added). The pellet was treated with a drop of mineral oil for index-matching to reduce light scattering (gray section of the trace).

TOC Graphics